PAPER

Pulling a folded polymer through a nanopore

IOP Publishing Journal of Physics: Condensed Matter
J. Phys.: Condens. Matter **33** (2020) 015101 (12pp) https://doi.org/10.1088/1361-648X/abb687

Pulling a folded polymer through a nanopore

Bappa Ghosh[1,5], Jalal Sarabadani[2,5,*], Srabanti Chaudhury[1,*] and Tapio Ala-Nissila[3,4]

[1] Department of Chemistry, Indian Institute of Science Education and Research, Pune, Maharashtra, India
[2] School of Nano Science, Institute for Research in Fundamental Sciences (IPM), 19395-5531, Tehran, Iran
[3] Department of Applied Physics and QTF Center of Excellence, Aalto University, PO Box 11000, FI-00076 Aalto, Espoo, Finland
[4] Interdisciplinary Centre for Mathematical Modelling and Department of Mathematical Sciences, Loughborough University, Loughborough, Leicestershire LE11 3TU, United Kingdom

E-mail: jalal@ipm.ir and srabanti@iiserpune.ac.in

Received 17 June 2020, revised 8 September 2020
Accepted for publication 9 September 2020
Published 7 October 2020

Abstract

We investigate the translocation dynamics of a folded linear polymer which is pulled through a nanopore by an external force. To this end, we generalize the iso-flux tension propagation theory for end-pulled polymer translocation to include the case of two segments of the folded polymer traversing simultaneously trough the pore. Our theory is extensively benchmarked with corresponding molecular dynamics (MD) simulations. The translocation process for a folded polymer can be divided into two main stages. In the first stage, both branches are traversing the pore and their dynamics is coupled. If the branches are not of equal length, there is a second stage where translocation of the shorter branch has been completed. Using the assumption of equal monomer flux of both branches confirmed by MD simulations, we analytically derive the equations of motion for both branches and characterize the translocation dynamics in detail from the average waiting time and its scaling form.

Keywords: translocation, folded polymer, nanopore, polymer dynamics

(Some figures may appear in colour only in the online journal)

1. Introduction

The process of polymer translocation through nanometer sized pores plays an important role in many biological [1, 2] as well as technological applications [3, 4]. Experiments using single molecule precision have stimulated many theoretical and computational studies on polymer translocation [5–31]. Over the last few years a comprehensive theory of driven translocation dynamics has been developed based on the idea of tension propagation (TP) in the chain. This iso-flux tension propagation (IFTP) theory has been applied to a variety of different physical scenarios [22], including pore-driven translocation of flexible [18] and semi-flexible [21] polymers, end-pulled [20] polymers, and translocation of a flexible polymer through a flickering nanopore under an alternating external driving force acting in the pore [19]. In the pore-driven case the monomers inside the pore experience the driving force due to an electric field caused by a voltage bias between the two membrane sides. On the other hand for the end-pulled case using a magnetic or an optical tweezers [32–38], or even an atomic force microscope [39] the polymer is pulled through a nanopore. Moreover, the end-pulled scenario is a promising method to control and slow down the translocation process that is crucial to properly identify the nucleotides in the sequencing of DNA [40–42].

Experiments on polymer translocation typically involve the electrically driven movement of charged polymers through pores whose typical diameters range from nanometers to tens of nanometers. In most of these experiments, the α-hemolysin pore complex is used in common to study the translocation

[5] These two authors contributed equally.
[*] Authors to whom any correspondence should be addressed.

process [1, 5, 43]. These experimental studies have been effective in distinguishing polymers of different molecular weights and sequences. However, there are several limitations in the use of this approach. The α-hemolysin pore has a diameter about 2 nm such that only single-stranded DNA/RNA molecules or synthetic polyelectrolytes are restricted to thread through these protein channels. In the experiment by Kasianowicz *et al*, the ionic current through the voltage biased α-hemolysin pore can detect the translocation of single-stranded molecules through the narrow pore under the influence of an external field [5]. In addition, α-hemolysin is not stable at wide experimental conditions such as high voltages ranges, temperatures, pH etc.

To overcome these difficulties, artificial solid-state nanopores have been developed and applied for studying polymer translocation. These nanopores can be tuned to larger diameters of 10–20 nm that allows translocation of double-stranded DNA molecules. Experiments on double-strand DNA translocation using silicon oxide nanopores have been reported by Dekker and coworkers [44–47]. Such synthetic pores have a lot of advantages over biological pores. For example, the synthetic pores are stable under experimental conditions such as high temperature, extreme voltage and pH values [48–52]. Since solid-state pores can have larger diameters, it has been observed experimentally that a polymer can undergo not only single file motion through the pore but also in different folded states [53]. The formation of double-stranded DNA hairpins undergoing voltage-driven translocation through nanopores located in synthetic membranes has been studied using coarse-grained Langevin dynamics of translocation [54]. So far most studies have focused on single file chain translocation through a nanopore. However, in the experiments with wide enough nanopores a few percent of the successful translocation events involve folded chains [53]. Thus, it is desirable to develop a theoretical understanding of folded polymer translocation dynamics. To this end, Kotsev and Kolomeisky have given a theoretical description of the pore-driven translocation dynamics of polymer with folded configurations using simple discrete stochastic models [55]. The translocation dynamics is considered as the motion of the folded segment of the chain through the channel followed by the motion of the linear part of the polymer. However, as shown in several papers [10, 13, 18–22] driven polymer translocation is controlled by tension front propagation and a proper theoretical treatment using the IFTP theory has not been done to date.

To this end, here we study the translocation dynamics of a *pulled* folded polymer through a nanopore [20] by generalizing the IFTP theory to include the simultaneous translocation of two polymer strands in the pore. The theory is benchmarked with molecular dynamics (MD) simulations. We consider both the symmetric case where the polymer is pulled in the middle monomer such that branches have equal lengths, and the asymmetric case with unequal branch lengths, as shown in figure 1. The details of the modified IFTP theory can be found in section 2 and the results are discussed in section 3. Finally, section 4 is devoted to present the summary and conclusions.

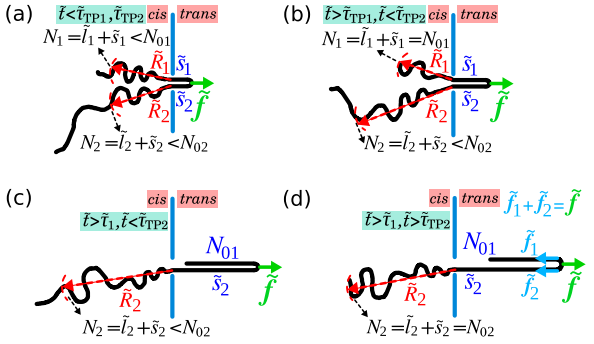

Figure 1. (a) Schematic of the translocation process of a polymer with a folded configuration. The contour lengths for the short and long branches are N_{01} and N_{02}, respectively. The external driving force, $\tilde{f}$, acts on the pulled monomer that connects the short branch to the longer one. The direction of the force is from the *cis* toward the *trans* side. For both branches the translocation process is in the TP stage (TP1–TP2), where the tension forces have not reached the branch ends. For each branch the location of the tension front separates the mobile part from the immobile equilibrium part, and is represented by $\tilde{R}_1$ and $\tilde{R}_2$ for the short and long branches, respectively. The number of translocated monomers (translocation coordinates) for the short and long branches are $\tilde{s}_1$ and $\tilde{s}_2$, respectively. (b) The translocation process is in the TP stage for the long branch while it is in post propagation stage for the short one, where the tension force has already reached the short branch end (PP1–TP2). (c) The translocation process for the short branch has been completed while it is still in the TP stage for the longer one (τ_1-TP2 stage, where τ_1 stands for the translocation time of the short branch). (d) The same as panel (c) but the translocation process is in the post propagation stage for the long branch (τ_1-PP2). Here, the contribution of the total external driving force, $\tilde{f}$, to each branch has been shown as $\tilde{f}_1$ and $\tilde{f}_2$ (not shown in panels (a)–(c)).

2. Theoretical model

In this section we generalize the IFTP theory for end-pulled translocation dynamics [20] to the present case of a folded linear polymer. When the contour lengths of both branches are the same, they traverse through the pore at equal rates on average. In contrast when the contour length of branches are not equal the translocation time of the shorter branch is less than that of the longer one. To develop the IFTP theory we consider here the high force limit and assume that the *trans* side sub-branches are fully straightened. This imposes the condition that the monomer flux which is the number of monomers that pass through the pore per unit time is the same for both branches. The dynamics of each branch is studied separately in the presence of the other one which leads to coupling between their equations of motion.

For the sake of simplicity, in the IFTP theory dimensionless units denoted by tilde are used as $\tilde{Y} \equiv Y/Y_u$, with the units of time $t_u \equiv \eta\sigma^2/(k_BT)$, length $s_u \equiv \sigma$, velocity $v_u \equiv \sigma/t_u = k_BT/(\eta\sigma)$, force $f_u \equiv k_BT/\sigma$, monomer flux $\phi_u \equiv k_BT/(\eta\sigma^2)$ and friction $\Gamma_u \equiv \eta$, where T is the temperature of the system, k_B is the Boltzmann constant, σ is the length of each segment, and the solvent friction coefficient per monomer is η. The quantities without the tilde are expressed in the Lennard-Jones units.

In figure 1 we show a schematic of the translocation process of a folded polymer. The contour lengths for the short and the long branches are denoted by N_{01} and N_{02}, respectively, i.e. $N_{01} \leqslant N_{02}$. The external driving force, $\tilde{f}$, acts on the monomer which connects the short branch to the longer one, and its direction is from *cis* toward the *trans* side. Panel (a) illustrates the TP stage for both branches, i.e. the TP1–TP2 stage, where the tension force has not reached the branch ends and $N_b = \tilde{l}_b + \tilde{s}_b < N_{0b}$ ($b = 1$ and 2 stand for the short and long branches, respectively). $N_{1(2)}$ is the total number of beads in branch 1(2) that have been already affected by the tension force, the number of translocated monomers (translocation coordinates) for the short and long branches are $\tilde{s}_1$ and $\tilde{s}_2$, respectively, and $\tilde{l}_{1(2)}$ is the number of beads in the mobile domain of the *cis* side sub-branch 1(2). In the TP stage the location of the tension front separates the mobile sub-branches from the immobile equilibrium ones, and is represented by $\tilde{R}_{1(2)}$ for branch 1(2). During the TP stage, as the equilibrium part of each branch is not aware of the tension force in its mobile domain due to symmetry $\tilde{R}_1 = \tilde{R}_2$, which is confirmed by the MD simulations in section 3.1. When both branches are inside the pore then $\tilde{s}_1 = \tilde{s}_2$. This is due to the strong force limit, wherein both sub-branches in the *trans* side are straightened. As time passes the short branch experiences the post propagation (PP1) stage, where the tension force has reached its end, and $N_1 = \tilde{l}_1 + \tilde{s}_1 = N_{01}$, while the longer one is still in the TP stage. The stage of this part of translocation process is called PP1–TP2, which is illustrated in panel (b). Then as can be seen in panel (c), the translocation process for the short branch has been completed while it is still in TP stage for the long branch. The abbreviation for this stage is τ_1-TP2, where τ_1 is the translocation time for the short branch. Finally, panel (d) shows that the translocation process is in post propagation (PP) stage for the long branch 2 with the abbreviation τ_1-PP2. Moreover, in panel (d), the contributions of the total external driving force, $\tilde{f}$, to branch 1 and 2 are illustrated as $\tilde{f}_1$ and $\tilde{f}_2$, respectively. The force balance for the pulled monomer gives $\tilde{f}_1 + \tilde{f}_2 = \tilde{f}$ (not shown in panels (a)–(c)).

In addition, in the very strong force limit of $\tilde{f}_{01(2)} > N_{1(2)}$ ($\tilde{f}_{01(2)}$ is the force on branch 1(2) at the entrance of the pore in the *cis* side and will be defined later) the mobile sub-branch 1(2) in the *cis* side is fully straightened, which is called the strong stretching (SS) limit. In the moderate external force limit of $1 < \tilde{f}_{01(2)} < N_{1(2)}$ the regime is called stem-flower (SF) as the shape of the mobile sub-branch 1(2) in the *cis* side is similar to a stem followed by a flower. Finally, the weak force limit of $\tilde{f}_{01(2)} < 1$ is called the trumpet (TR) regime, where the mobile sub-branch 1(2) in the *cis* side assumes a TR shape [20, 56].

As mentioned above and depicted in figure 1 only the SS regime in the *trans* side is considered here, and therefore using the deterministic version of the iso-flux (IF) Brownian dynamics TP theory without any entropic force [13, 18] is a very good approximation. Within this framework, in the TP1–TP2 and PP1–TP2 stages (panels (a) and (b) in figure 1) the equations of motion for the time evolution of the translocation coordinates (the number of translocated beads to the *trans* side) $\tilde{s}_1$ and $\tilde{s}_2$ for branch 1 (short) and branch 2 (long), respectively, are coupled to each other and written as

$$\begin{cases} \tilde{\Gamma}_1(\tilde{t}) \left(\mathrm{d}\tilde{s}_1/\mathrm{d}\tilde{t}\right) = \tilde{f}_1, & \text{for branch 1;} \\ \tilde{\Gamma}_2(\tilde{t}) \left(\mathrm{d}\tilde{s}_2/\mathrm{d}\tilde{t}\right) = \tilde{f}_2, & \text{for branch 2,} \end{cases} \tag{1}$$

where $\tilde{\Gamma}_b(\tilde{t})$ ($b = 1$ and 2 stand for short and long branches, respectively) is the effective friction and $\tilde{f}_b$ is the contribution of the total external driving force $\tilde{f}$ to branch b as depicted in figure 1(d). According to references [20, 21] the effective friction can be obtained as $\tilde{\Gamma}_b(\tilde{t}) = \tilde{\eta}_{\mathrm{cis}b}(\tilde{t}) + \tilde{\eta}_{\mathrm{p}} + \tilde{\eta}_{\mathrm{TS}b}(\tilde{t})$, where $\tilde{\eta}_{\mathrm{cis}b}(\tilde{t})$ denotes the friction due the *cis* side mobile sub-branch b in the solvent, $\tilde{\eta}_{\mathrm{p}}(\tilde{t})$ is the pore friction, and $\tilde{\eta}_{\mathrm{TS}b}(\tilde{t})$ presents the friction due the movement of the *trans* side (TS) mobile sub-branch b. When both branches are inside the pore (panels (a) and (b) in figure 1), the pore friction is $\tilde{\eta}_{\mathrm{p}} = \tilde{\eta}_{\mathrm{p}12}$ and when only the longer one (branch 2) is inside the pore (panels (c) and (d) in figure 1), $\tilde{\eta}_{\mathrm{p}} = \tilde{\eta}_{\mathrm{p}2}$ is the pore friction. It should be mentioned that the *trans* side friction terms play an important role in the dynamics of the current system [20, 21]. This will be discussed in detail below. Later it will be shown how to find the values of $\tilde{f}_1$ and $\tilde{f}_2$ during the translocation process. In the symmetric case when the contour lengths of both branches are the same, i.e. $N_{01} = N_{02}$, then due to the symmetry of the system $\tilde{f}_1 = \tilde{f}_2 = \tilde{f}/2$ during the whole translocation process.

Using the IFTP theory the dynamics of each branch in the *cis* and in the *trans* sides is separately solved with the corresponding TP equations. The IF approximation is used to find the TP equations [56]. In the IF approximation the monomer flux $\tilde{\phi}_b(\tilde{t}) = \mathrm{d}\tilde{s}_b/\mathrm{d}\tilde{t}$ ($b = 1$ or 2) within the mobile domain for each branch is constant in space but evolves with time. In the TP1–TP2 and PP1–TP2 stages (panels (a) and (b) in figure 1, respectively) the tension front for branch b is located at distance $\tilde{x} = \tilde{R}_b(\tilde{t})$ to the pore in the *cis* side. Inside each branch, the tension force is mediated from the pulled monomer at the distance $\tilde{s}_b$ in the *trans* side all the way to the pore located at $\tilde{x} = 0$ and then to the last mobile bead N_b located in the tension front in the *cis* side. Performing the integration of the local force-balance relation $\mathrm{d}\tilde{f}_b(\tilde{x}') = -\tilde{\phi}_b(\tilde{t})\mathrm{d}\tilde{x}'$ [18, 20] over the distance from the location of the pulled monomer to $\tilde{x}$, gives the tension force at the distance $\tilde{x}$ as

$$\tilde{f}_b(\tilde{x}, \tilde{t}) = \tilde{f}_{0b} - \tilde{x}\tilde{\phi}_b(\tilde{t}), \tag{2}$$

where $\tilde{f}_{0b} = \tilde{f}_b - \tilde{\eta}_{\mathrm{p}}\tilde{\phi}_b(\tilde{t}) - \tilde{\eta}_{\mathrm{TS}b}\tilde{\phi}_b(\tilde{t})$ is the force at the entrance of the pore in the *cis* side. Combining equation (2) and the fact that the tension force vanishes at the tension front, i.e. $\tilde{f}_b(\tilde{R}_b, \tilde{t}) = 0$ yields the monomer flux as

$$\tilde{\phi}_b(\tilde{t}) = \frac{\tilde{f}_b}{\tilde{R}_b + \tilde{\eta}_{\mathrm{p}} + \tilde{\eta}_{\mathrm{TS}b}}. \tag{3}$$

Since we are in the SS limit for both sub-branches in the *trans* side, $\tilde{\eta}_{\mathrm{TS}b} = \tilde{s}_b = \tilde{s}$. Moreover, as mentioned above when both branches are inside the pore $\tilde{\eta}_{\mathrm{p}} = \tilde{\eta}_{\mathrm{p}12}$, and if only the long branch is located in the pore $\tilde{\eta}_{\mathrm{p}} = \tilde{\eta}_{\mathrm{p}2}$.

To determine $\tilde{f}_1$ and $\tilde{f}_2$, two equations must be solved. The first equation is $\tilde{f}_1 + \tilde{f}_2 = \tilde{f}$, which is the force balance equation for the pulled monomer as shown in figure 1(d). The

second one comes from the fact that monomer fluxes for both branches are the same, i.e. $\tilde{\phi}_1(\tilde{t}) = \tilde{\phi}_2(\tilde{t})$, where $\tilde{\phi}_b(\tilde{t})$ has been defined in equation (3). Solving these two equations gives

$$\begin{aligned}\tilde{f}_1 &= \tilde{f} \times \left(1 + \frac{\tilde{R}_2 + \tilde{\eta}_{\mathrm{TS2}} + \tilde{\eta}_{\mathrm{p12}}}{\tilde{R}_1 + \tilde{\eta}_{\mathrm{TS1}} + \tilde{\eta}_{\mathrm{p12}}}\right)^{-1},\\ \tilde{f}_2 &= \tilde{f} \times \left(1 + \frac{\tilde{R}_1 + \tilde{\eta}_{\mathrm{TS1}} + \tilde{\eta}_{\mathrm{p12}}}{\tilde{R}_2 + \tilde{\eta}_{\mathrm{TS2}} + \tilde{\eta}_{\mathrm{p12}}}\right)^{-1}.\end{aligned} \tag{4}$$

Inserting the above $\tilde{f}_b$ into equation (3), the monomer flux reads

$$\tilde{\phi}_1(\tilde{t}) = \tilde{\phi}_2(\tilde{t}) = \tilde{\phi}(\tilde{t}) = \frac{\tilde{f}}{\tilde{R}_1 + \tilde{R}_2 + 2\tilde{\eta}_{\mathrm{p12}} + \tilde{\eta}_{\mathrm{TS1}} + \tilde{\eta}_{\mathrm{TS2}}}. \tag{5}$$

If the contour lengths for both branches are the same, or the translocation process is in the TP1–TP2 stage as depicted in figure 1(a), then due to the symmetry $\tilde{R}_1 = \tilde{R}_2$. This leads to $\tilde{f}_1 = \tilde{f}_2 = \tilde{f}/2$, and consequently $\tilde{\phi}_1(\tilde{t}) = \tilde{\phi}_2(\tilde{t}) = \tilde{\phi}(\tilde{t}) = (1/2)\tilde{f} \times \left(\tilde{R} + \tilde{\eta}_{\mathrm{p12}} + \tilde{s}\right)^{-1}$.

In the τ_1-TP2 and τ_1-PP2 stages (panels (c) and (d) in figure 1), where the whole short branch has been translocated to the *trans* side and $\tilde{s}_1 = N_{01}$, only branch 2 is inside the nanopore and the time evolution of $\tilde{s}_2$ is given by

$$\tilde{\Gamma}_2(\tilde{t})\ \frac{\mathrm{d}\tilde{s}_2}{\mathrm{d}\tilde{t}} = \tilde{f}_2. \tag{6}$$

Using the force balance equation for the pulled monomer together with the fact that the tension force vanishes at the last monomer of branch 1 in the *trans* side (panels (c) and (d) in figure 1) gives

$$\begin{aligned}\tilde{f}_1 &= \frac{\tilde{f} \times N_{01}}{\tilde{R}_2 + \tilde{s}_2 + N_{01} + \tilde{\eta}_{\mathrm{p2}}},\\ \tilde{f}_2 &= \frac{\tilde{f} \times \left(\tilde{R}_2 + \tilde{s}_2 + \tilde{\eta}_{\mathrm{p2}}\right)}{\tilde{R}_2 + \tilde{s}_2 + N_{01} + \tilde{\eta}_{\mathrm{p2}}},\end{aligned} \tag{7}$$

where as mentioned above $\tilde{\eta}_{\mathrm{p2}}$ is the pore friction when only the long branch 2 is inside the pore, and N_{01} is the *trans* side friction due to the whole mobile short branch 1. Then the monomer flux for the long branch is cast into

$$\tilde{\phi}_2(\tilde{t}) = \frac{\tilde{f}}{\tilde{R}_2 + \tilde{\eta}_{\mathrm{p2}} + \tilde{s}_2 + N_{01}}. \tag{8}$$

In the TP1–TP2 and PP1–TP2 stages (panels (a) and (b) in figure 1) combining equations (1), (3) and (4), the time evolution of the translocation coordinates are obtained for short ($\tilde{s}_1$) and long ($\tilde{s}_2$) branches provided that the time evolution of the location of the tension front for each branch is known. On the other hand in the τ_1-TP2 and τ_1-PP2 stages (panels (c) and (d) in figure 1), where the the translocation process for the short branch 1 has already terminated, equations (6) and (7) together with equation (8) give the translocation coordinate for the longer branch ($\tilde{s}_2$) as a function of time again if the location of the tension front for the long branch is know. Therefore, to proceed further the time evolution of the location of the tension fronts for the short as well as long branches, $\tilde{R}_1$ and $\tilde{R}_2$, should be obtained.

To obtain the time evolution of $\tilde{R}_1$ and $\tilde{R}_2$ (the distances between the nanopore and the locations of the tension fronts for branches 1 and 2, respectively,) in the TP1–TP2 stage in panel (a) in figure 1, and $\tilde{R}_2$ in the TP2 stage in panel (b) in figure 1 on the *cis* side, one can use the end-to-end distance that corresponds to the size of the mobile sub-branches at equilibrium just before translocation process. Here we consider the end-to-end distance for sub-branch 1. The same procedure is applied for the long branch. To understand why $\tilde{R}_1$ is the same as the end-to-end distance $\tilde{R}_{\mathrm{e}}$, one needs to compare the polymer configuration in its equilibrium state just before starting the translocation process at time zero with the chain configuration at time $\tilde{t}$. Looking at the polymer configuration at time $\tilde{t}$ the number of the monomers affected by the tension by the time $\tilde{t}$ is written as N_1, where $N_1 = \tilde{l}_1 + \tilde{s}_1$ is the total number of mobile monomers for sub-branch 1, $\tilde{l}_1$ is the number of mobile monomers in the *cis* side belonging to sub-branch 1 and $\tilde{s}_1$ is the number of mobile monomers that have already traversed the pore and are in the *trans* side. On the other hand at time $\tilde{t} = 0$ the number of monomers accommodated in the space between the nanopore and the tension front (at time $\tilde{t}$) is the same as N_1. Moreover, at time $\tilde{t} = 0$, where the system is in its equilibrium state, the size of the sub-chain with the contour length of N_1 occupying the space between the nanopore and the tension front (at time $\tilde{t}$) is determined by its end-to-end distance, which is given by Flory theory as $\tilde{R}_{\mathrm{e}} = A_\nu N_1^\nu$, where $A_\nu = 1.15$ is a constant obtained from MD simulations and $\nu \approx 0.588$ is the Flory exponent in 3D. Therefore, as the distance between the location of the tension front and the nanopore at time $\tilde{t}$ is the same as the end-to-end distance of the sub-chain with the contour length of N_1 at time $\tilde{t} = 0$, one can simply write $\tilde{R}_1 = \tilde{R}_{\mathrm{e}} = A_\nu N_1^\nu = A_\nu(\tilde{l}_1 + \tilde{s}_1)^\nu$.

The time derivative of the above relation is then written as $\dot{\tilde{R}}_1 = A_\nu^{1/\nu}\tilde{R}_1^{(\nu-1)/\nu}\left(\dot{\tilde{l}}_1 + \dot{\tilde{s}}_1\right)$, where $\dot{\tilde{s}}_1$ is the monomer flux $\tilde{\phi}_1$, and $\dot{\tilde{l}}_1$ must be found. In the SS and stem part of the SF regimes as the mobile sub-branch 1 in the *cis* side is fully straightened the monomer number density is unity, while according to the blob theory in the flower part of the SF and TR regimes the monomer number density is written as $\tilde{\sigma}_1(\tilde{x}) = |\tilde{f}_1(\tilde{x})|^{(\nu-1)/\nu}$, where $\tilde{f}_1(\tilde{x})$ is the tension force at the distance $\tilde{x}$ from the pore in the *cis* side and given by equation (2), and is larger than unity due to polymer folding inside the existing blobs. Indeed, following the Pincus blob theory [57] as the *cis* side sub-chain 1 is under tension there exist blobs with increasing radii, $\tilde{\xi}_1(\tilde{x}) = 1/|\tilde{f}_1(\tilde{x})|$, when getting away from the pore (since according to equation (2) the value of the tension force $\tilde{f}_1(\tilde{x})$ decreases with increasing $\tilde{x}$). To find the monomer number density one needs to consider the monomers inside each blob, wherein the chain is not disturbed by the tension force and according to Flory theory the blob size is given by $\tilde{\xi}_1(\tilde{x}) \sim g_1^\nu$, where g_1 is the number of beads inside the blob. Then the monomer number density is obtained as $\tilde{\sigma}_1(\tilde{x}) = g_1/\tilde{\xi}_1(\tilde{x}) = \tilde{\xi}_1(\tilde{x})^{1/\nu-1} = |\tilde{f}_1(\tilde{x})|^{1-1/\nu}$. To find the number of mobile monomers in the *cis* side $\tilde{l}$ the monomer number density $\tilde{\sigma}_1(\tilde{x})$ is integrated

over the distance from the pore entrance in the *cis* side to the location of the tension front $\tilde{R}_1$ in the SS, SF and TR regimes as $\tilde{l}_1 = \int_{\tilde{x}=0}^{\tilde{x}=\tilde{R}_1} \tilde{\sigma}_1(\tilde{x})\mathrm{d}\tilde{x} = \int_{\tilde{x}=0}^{\tilde{x}=\tilde{R}_1} |\tilde{f}_1(\tilde{x})|^{1-1/\nu}\, \mathrm{d}\tilde{x}$ [18]. Then the number of mobile monomers belonging to branch 1 in the *cis* side is written as

$$\begin{aligned} \tilde{l}_1 &= \tilde{R}_1, \quad \text{in the SS regime;} \\ \tilde{l}_1 &= \tilde{R}_1 + \frac{1-\nu}{2\nu-1}\frac{1}{\tilde{\phi}_1}, \quad \text{in the SF regime;} \\ \tilde{l}_1 &= \frac{\nu}{2\nu-1}\tilde{R}_1^{(2\nu-1)/\nu}\tilde{\phi}_1^{(\nu-1)/\nu}, \quad \text{in the TR regime.} \end{aligned} \tag{9}$$

To obtain $\tilde{l}_2$ the subscripts 1 in equation (9) must be replaced by 2. Substituting the time derivative of $\tilde{l}_1$ in the relation $\dot{\tilde{R}}_1 = A_\nu^{1/\nu}\tilde{R}_1^{(\nu-1)/\nu}\left(\dot{\tilde{l}}_1 + \dot{\tilde{s}}_1\right)$, together with the fact that $\dot{\tilde{s}}_1 = \tilde{\phi}_1$, the equation of motion for $\tilde{R}_1$ when both branches are inside the pore in the TP stage is obtained.

In the PP stage, wherein the last bead of the chain in the *cis* side has been already influenced by the tension, the closure relation for branch 1 is $N_1 = \tilde{l}_1 + \tilde{s}_1 = N_{01}$, where the right-hand side is the total contour length of branch 1 which is constant. Performing the time derivative of both sides of the closure relation, $\tilde{l}_1 + \tilde{s}_1 = N_{01}$, gives $\dot{\tilde{l}}_1 = -\tilde{\phi}_1$. Finally, to obtain the time evolution of tension front location in the different regimes of SS, SF and TR, $\tilde{l}_1$, which is obtained from equation (9), must be replaced in $\dot{\tilde{l}}_1 = -\tilde{\phi}_1$. Similar procedure is employed for the long branch 2 in order to find the equation for the time evolution of the tension front $\tilde{R}_2$.

Then the coupled equations of motion for the location of tension fronts for short branch 1 and for long branch 2 are cast into

$$\begin{aligned} \dot{\tilde{R}}_1 &= \mathcal{U}_1^{\mathrm{I,J}}, \quad \mathrm{I} = \text{SS, SF or TR regime, and J} = \text{TP or PP stage;} \\ \dot{\tilde{R}}_2 &= \mathcal{U}_2^{\mathrm{I,J}}, \quad \mathrm{I} = \text{SS, SF or TR regime, and J} = \text{TP or PP stage.} \end{aligned} \tag{10}$$

As depicted in figures 1(c) and (d), when the translocation process has already terminated for the short branch 1 and only the longer branch 2 is traversing the nanopore the same procedure is repeated to obtain the equation of motion for the location of tension front for the long branch 2. Then the equation of motion for the location of the tension front for branch 2 is

$$\dot{\tilde{R}}_2 = \mathcal{V}_2^{\mathrm{I,J}}, \quad \mathrm{I} = \text{SS, SF or TR regime, and J} = \text{TP or PP stage.} \tag{11}$$

It should be mentioned that $\tilde{\mathcal{U}}_{1(2)}^{\mathrm{I,J}}$ are functions of ν, A_ν, $\tilde{R}_1$, $\tilde{R}_2$, $\tilde{s}_1$, $\tilde{s}_2$, $\tilde{\eta}_{\mathrm{p}12}$ and $\tilde{f}$, while $\tilde{\mathcal{V}}_2^{\mathrm{I,J}}$ is function of ν, A_ν, $\tilde{R}_2$, $\tilde{s}_2$, $\tilde{\eta}_{\mathrm{p}2}$, N_{01} and $\tilde{f}$, and their explicit forms can be found in appendix A.

To have the full solution of the IFTP model when both branches are passing through the pore equations (1), (5) and (10) should be solved self-consistently, and when only the long branch remains one must solve equations (6)–(8) and (11).

3. Results

3.1. Waiting time distribution

In order to examine the validity of the IFTP theory we first compare dynamics of the translocation process at the monomer level between IFTP theory and MD simulations using the waiting time distribution (WT), which is the average time that each bead spends in the pore during the process of the translocation. The details of the MD simulation method are presented in appendix B. In figure 2 we show our data for the three sets of folded polymers. In panel (a) the WT $w(\tilde{s})$ has been plotted as a function of the translocation coordinate $\tilde{s}$ for the case wherein the branches have the same contour length, i.e. $N_{01} = N_{02} = 51$, with the total contour length of linear polymer $N_0 = N_{01} + N_{02} = 101$. Here the bead that connects the two branches naturally belongs to both of them. The pore friction used in the IFTP theory is $\eta_{\mathrm{p}12} = 6$, external driving force which acts on the connecting bead is $f = 100$ (both in the theory as well as in the MD simulations) and $k = 30$ is the spring constant in the bead-spring model used in the MD simulations. Open light blue circles and open orange triangles are MD data while the solid red line represents the IFTP theory results. Panels (b) and (c) are the same as (a) but for different values of the contour lengths of the two branches $N_{01} = 31$ and $N_{02} = 71$, and $N_{01} = 11$ and $N_{02} = 91$, respectively, with constant $N_0 = 101$. In panels (b) and (c) when both branches are traversing the pore, the pore friction in the IFTP theory is chosen as $\eta_{\mathrm{p}12} = 6$, and after the translocation of the short branch when only branch 2 is traversing the nanopore it reduces to the fixed value of $\eta_{\mathrm{p}2} = 3$. Open light blue circles and open orange triangles are MD data for short and long branches, respectively, while the solid blue and the dashed red lines represent the IFTP theory results for the short and long branches, respectively. It is obvious from the figure that the agreement between IFTP theory and MD simulations is very good. Interestingly, in figure 2 MD simulations data match the IFTP theory results, which reveals that during the TP1–TP2 stage (panel (a) in figure 1) as expected from symmetry, the size of the mobile parts of the short and long branches are the same, i.e. $\tilde{R}_1 = \tilde{R}_2$.

It should be mentioned that during the translocation process, the tension is propagating on both branches of the folded chain and there is an increase in the WT due to an increase in the effective friction. The effective friction originates from the moving part of the chain as well as the pore friction. The increase in the WT continues till the tension reaches the last bead of each branch. For unequal branches, when the translocation process terminates for the shorter one, there exists only one monomer inside the pore resulting in decrease of the effective pore-friction which is reflected on the sudden drop of the WT curve for the shorter branch. With further increase in $\tilde{s}$, the tension continues to propagate on the longer chain, and at large values of $\tilde{s}$, when the tension reaches the last bead of the longer branch, the TP completes, and the whole branch becomes mobile. Therefore, there is no further increase of effective friction and the WT

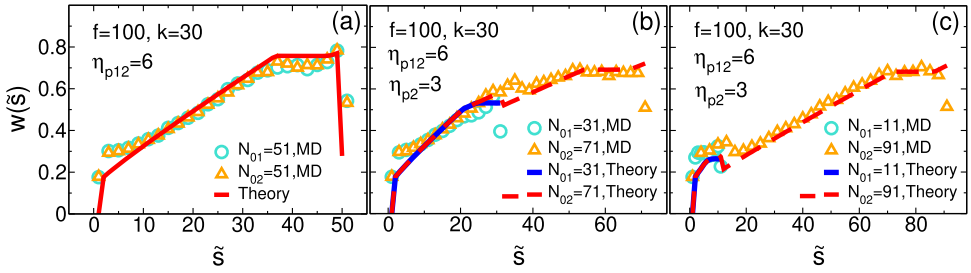

Figure 2. (a) The waiting time distribution $w(\tilde{s})$ as a function of the translocation coordinate $\tilde{s}$ for the folded linear polymer chain with equal branches, i.e. $N_{01} = N_{02} = 50 + 1$, with $N_0 = N_{01} + N_{02} = 101$, pore friction $\eta_{p12} = 6$, external driving force $f = 100$ and spring constant $k = 30$ in the bead-spring model used in the MD simulations. Open light blue circles and open orange triangles are MD data while the solid red line represents the IFTP theory results. Panels (b) and (c) are the same as panel (a) but for different values of the contour lengths of the two branches $N_{01} = 31$ and $N_{02} = 71$, and $N_{01} = 11$ and $N_{02} = 91$, respectively, with constant $N_0 = 101$. In panels (b) and (c) $\eta_{p12} = 6$ and $\eta_{p2} = 3$ are the pore frictions, when both branches are in the pore and after the translocation of the short branch to the *cis* side, respectively. Open light blue circles and open orange triangles are MD data for the short and long branches, respectively, while the solid blue and the dashed red lines represent the IFTP theory results for the short and long branches, respectively.

gets almost constant value, as shown in panels (b) and (c) in figure 2.

Finally, we would like to stress the fact that the theory presented here has only one unknown parameter $\tilde{\eta}_{p2}$, which is determined by comparing the WT coming from the IFTP theory with the one from MD. This allows us to set the value of this fitting parameter as $\tilde{\eta}_{p2} = 3$ for the present pore geometry and interactions. For the folded chain we then simply use twice the value of the single-chain pore friction, i.e. $\tilde{\eta}_{p12} = 6$.

3.2. Translocation time for each branch

The central quantity that describes the global dynamics of the polymer translocation through a nanopore is the average translocation time $\tilde{\tau}$. To find the IFTP translocation time for the short and long branches, τ_1 and τ_2, respectively, equations (1), (5)–(8), (10) and (11) must be solved self-consistently. To compare with MD, in figure 3 the normalized translocation time for the short branch $\tau_1/\tau_1(N_{01} = 51)$ has been plotted as a function of the contour length of the short branch N_{01}, while the normalized translocation time for the long branch $\tau_2/\tau_2(N_{02} = 51)$, has been plotted as a function of the contour length of the longer branch N_{02}. The data the for short branch must be read from left and bottom blue axes, while for the long branch from the right and top red axes. $\tau_1(N_{01} = 51) = \tau_2(N_{02} = 51)$ are the translocation times for the two branches of a folded linear polymer with contour length of $N_0 = 101$ when the polymer is folded in the middle. For the short branch the light blue open circles present the MD data, and the solid blue line shows the IFTP theory results. On the other hand the open orange triangles and the solid red line present the MD and the IFTP theory results, respectively, for the long branch. As the figure shows the data are in excellent agreement as already expected from the WT distributions.

3.3. Scaling of the translocation time

To find a scaling form for the translocation time for the short branch equation (5) should be integrated over N_1 from zero to N_{01} in the TP1–TP2 stage as depicted in figure 1(a) followed

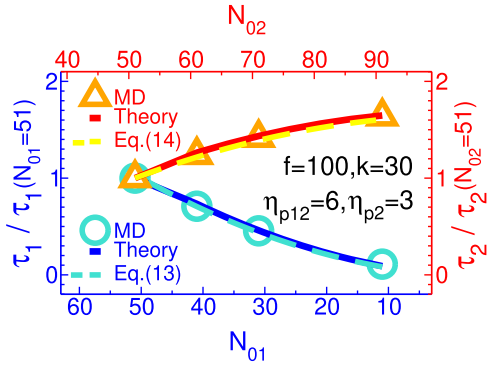

Figure 3. Normalized translocation time $\tau_1/\tau_1(N_{01} = 51)$ as a function of the contour length for the short branch N_{01}, and $\tau_2/\tau_2(N_{02} = 51)$ as a function of the contour length for the long branch N_{02}. For the short branch the light blue open circles present the MD data, and the solid blue line shows the IFTP theory results. For the long branch the open orange triangles and the solid red line present the MD and IFTP theory results, respectively. The data for the short branch must be read from the bottom horizontal and left vertical blue axes, while for the long branch the data should be read from the top horizontal and right vertical red axes. The results of the equations (12) and (13) are shown in light blue dashed and yellow dashed lines for the short and long branches, respectively.

by the integration of $\tilde{R}_1$ from $\tilde{R}_1(N_{01})$ to zero in the PP1–TP2 stage as shown in figure 1(b). This yields the translocation time for the short branch in the SS regime for the *cis* and *trans* sides as

$$\tilde{\tau}_1 = \frac{1}{\tilde{f}/2}\left(\frac{A_\nu}{1+\nu}\, N_{01}^{1+\nu} + \frac{N_{01}^2}{2} + \tilde{\eta}_{p12}\, N_{01}\right), \qquad (12)$$

where the first, second and the third terms in the rhs of equation (12) are due to the mobile sub-branch friction in the *cis* side, straightened sub-chain friction in the *trans* side and the pore friction, respectively. Similarly, to find a closed form of the translocation time for the longer branch in the SS regime, one needs to integrate equation (8) over N_2 from N_{01} to N_{02} in the τ_1-TP2 stage as presented in figure 1(c) followed by the integration of $\tilde{R}_2$ from $\tilde{R}_2(N_{02})$ to zero in the τ_1-PP2 stage as

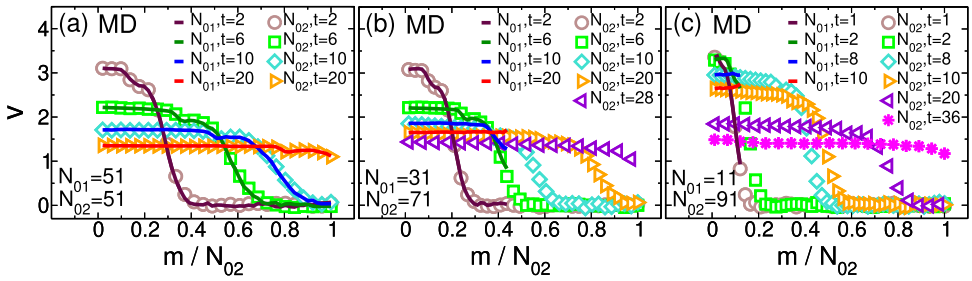

Figure 4. (a) The velocities of the individual monomers from MD simulations as a function of the normalized monomer index, m/N_{02}, at different moments $t = 2$–20 for the symmetric folded chain with $N_{01} = N_{02} = 51$. Open symbols show the velocities for the branch 2, while the solid lines present the monomer velocities of the branch 1. Panels (b) and (c) are the same as panel (a) but for asymmetrical folded polymer chain with branch contour lengths $N_{01} = 31$ and $N_{02} = 71$, and $N_{01} = 11$ and $N_{02} = 91$, respectively. In panels (b) and (c) the label of the horizontal axis has been normalized to the contour length of the longer branch N_{02}, and the data are presented during $t = 2$–28 and $t = 1$–36, respectively.

shown in figure 1(d). Following this procedure the translocation time for the longer branch in the SS regime for the *cis* and *trans* sides can be written as

$$\tilde{\tau}_2 = \frac{1}{\tilde{f}}\left[+\frac{A_\nu}{1+\nu}\,N_{01}^{1+\nu} + \frac{A_\nu}{1+\nu}\,N_{02}^{1+\nu} + \frac{N_{02}^2}{2} - \frac{N_{01}^2}{2} + 2\tilde{\eta}_{\mathrm{p}12}\,N_{01} + \tilde{\eta}_{\mathrm{p}2}\,(N_{02}-N_{01}) + N_{01}N_{02}\right], \qquad (13)$$

revealing how the contour lengths of the short and long branches are coupled to each other. In figure 3 the results from the equations (12) and (13) are shown in light blue dashed and yellow dashed lines for the short and long branches, respectively. As can be seen there is a very good agreement between the normalized scaling formula, the MD results and the full IFTP theory, although the scaling formulae in equations (12) and (13) have been obtained in the limit of long branches in the SS regime.

4. Summary and conclusion

In this work, we have theoretically and computationally studied the translocation dynamics of a singly-folded polymer chain pulled through a nanopore by applying a pulling force on the monomer connecting the two branches. The pulling force initiates a tension front that propagates though the folds during translocation. To properly treat this, we have generalized the IFTP theory to the present case. The novelty of this work is that in the current version of the IFTP theory the equations for the time evolution of the translocation coordinates of both branches are coupled to each other through the assumption of the equality of the monomer fluxes of the branches at the pore. This leads to the coupling of the contour lengths of the shorter branch as well as the longer one in the translocation time for the longer branch in equation (13). The modified IFTP theory allows a proper treatment of folded polymer translocation here.

We have also performed extensive MD simulations of a coarse-grained bead-spring model to benchmark the theory. The WT distribution obtained from the IFTP theory has been compared with MD one showing good agreement at the monomer level dynamics. Then, the global dynamics of the translocation has been examined by looking at the translocation time for each branch obtained from the IFTP theory and MD simulations. Again the results of the IFTP theory are in excellent agreement with the MD simulations. We have also analytically derived scaling forms for the average translocation time from the IFTP theory showing explicitly how the two branches are dynamically coupled. For both branches the effective translocation exponent, α, which is defined as $\tau \sim N_{0b}^{\alpha}$ ($b = 1$ and 2 stand for short and long branches, respectively), is between 1 and 2. While α for the short branch depends on N_{01} (see equation (12)), for the long branch the translocation exponent depends on the values of both contour lengths N_{01} and N_{02} (see equation (13)).

Finally, we have used MD simulations presented in detail in appendix B, to characterize the velocities of the individual monomers for both branches (the details for monomers' velocities can be found in appendix C). As can be seen there the velocities of the individual monomers of both branches (for different sets of branch lengths) coincide with each other. This confirms that the assumption of equality of monomer fluxes for both branches at the pore in the IFTP theory is valid in the high force limit where in the *trans* side sub-branches are both in the SS regime. Moreover, appendix D is devoted to the study of the probability distribution of the translocation time. As the system becomes more asymmetrical, i.e. one branch gets shorter while the other one becomes longer, the probability distributions of the translocation time distributions for the short and long branches separate. In addition, the width of the distribution becomes narrower for the short branch.

Finally, it should be mentioned that when both sub-chains in the *trans* side are fully straightened (SS regime) the monomer fluxes $\tilde{\phi}$ for both branches are the same which has been confirmed by the MD simulations (see figure 4). Therefore, at all moments during the translocation process $\tilde{\phi}_1 = \tilde{\phi}_2$ and the branches do not drag each other inside the pore. On the other hand if the pulling force is not strong enough, then for the case of branches with unequal contour lengths one sub-chain in the *trans* side would be in one regime while the other one would be in a different regime. Therefore, this mixture of the regimes for different branches introduces unequal monomer fluxes for different branches that leads to a drag of one branch by the other

one inside the pore. In this situation the IFTP theory should be modified accordingly, which is beyond the scope of the present work.

Acknowledgments

SC and BG acknowledge DAE-BRNS (37(2)/14/08/2016-BRNS/37022) for computer facilities. BG acknowledges DAE-BRNS (37(2)/14/08/2016-BRNS/37022) and IISER Pune for fellowship. T A-N has been supported in part by the Academy of Finland through its PolyDyna (No. 307806) and QFT Center of Excellence Program Grants (No. 312298). JS thanks Takahiro Sakaue for enlightening discussions.

Appendix A

In this appendix the explicit forms of $\tilde{\mathcal{U}}_1^{\mathrm{I,J}}$ and $\tilde{\mathcal{U}}_2^{\mathrm{I,J}}$, which are functions of ν, A_ν, $\tilde{R}_1$, $\tilde{R}_2$, $\tilde{s}_1$, $\tilde{s}_2$, $\tilde{\eta}_{\mathrm{p}12}$ and $\tilde{f}$, and $\tilde{\mathcal{V}}_2^{\mathrm{I,J}}$ that is function of ν, A_ν, $\tilde{R}_2$, $\tilde{s}_2$, $\tilde{\eta}_{\mathrm{p}2}$, N_{01} and $\tilde{f}$ are given. While superscript I denotes different regimes of SS, SF or TR in the *cis* side, the superscript J is devoted to the TP or PP stages. To clarify why we need to present the equations of motion for $\tilde{R}_1$ and $\tilde{R}_2$ in the different regimes of SS, SF and TR, it should be mentioned that the condition to have the SS regime in the *trans* side sub-chain during the translocation process is $\tilde{f}_b > \tilde{s}_b$, where $b = 1$ and 2 indicates branch b. Indeed when the whole sub-chain b is mobile the condition is $\tilde{f}_b > N_{0b}$. On the other hand, the pore friction plays a role in the dynamics of the translocation chain in the *cis* side and as explained in the main text of the paper the conditions to have the SS, SF or TR regimes in the *cis* side are $\tilde{f}_{01(2)} > N_{1(2)}$, $1 < \tilde{f}_{01(2)} < N_{1(2)}$ or $\tilde{f}_{01(2)} < 1$, respectively, where $\tilde{f}_{01(2)} = \tilde{f}_{0b} - \tilde{x}\tilde{\phi}_b(\tilde{t})$ with $\tilde{f}_{0b} = \tilde{f}_b - \tilde{\eta}_{\mathrm{p}}\tilde{\phi}_b(\tilde{t}) - \tilde{\eta}_{\mathrm{TSb}}\tilde{\phi}_b(\tilde{t})$, is the force on branch 1(2) at the entrance of the pore in the *cis* side. This reveals that although the *trans* side sub-chains 1 and 2 are in the SS regime, in the *cis* side they can be in the SS, SF or TR regimes or in a mixture of them. Therefore, the equations of motion for $\tilde{R}_1$ and $\tilde{R}_2$ must be solved in the corresponding regimes.

The equations of motion for branches 1 and 2 are coupled to each other when both branches are traversing the nanopore and are written as

$$\begin{aligned}
&\dot{\tilde{R}}_1 = \mathcal{U}_1^{\mathrm{I,J}}, \quad \mathrm{I} = \mathrm{SS, SF\ or\ TR\ regime, and\ J} = \mathrm{TP\ or\ PP\ stage;}\\
&\dot{\tilde{R}}_2 = \mathcal{U}_2^{\mathrm{I,J}}, \quad \mathrm{I} = \mathrm{SS, SF\ or\ TR\ regime, and\ J} = \mathrm{TP\ or\ PP\ stage.}
\end{aligned} \tag{14}$$

As mentioned in section 2 when the translocation process for both branches is in the TP stage, i.e. in the TP1–TP2 stage (figure 1(a)), or the contour lengths for both branches are the same, then due to the symmetry $\tilde{R}_1 = \tilde{R}_2$. This leads to $\tilde{f}_1 = \tilde{f}_2 = \tilde{f}/2$. Therefore, the equations of motion for the location of the tension fronts for branches 1 and 2 are similar, and $\tilde{\mathcal{U}}_1^{\mathrm{I,J}}$ and $\tilde{\mathcal{U}}_2^{\mathrm{I,J}}$ are

$$\begin{aligned}
&\mathcal{U}_1^{\mathrm{SS,TP}} = \mathcal{U}_2^{\mathrm{SS,TP}} = \frac{B(\tilde{R}_b)\tilde{\phi}_b}{1 - B(\tilde{R}_b)}, \quad b = 1 \text{ or } 2;\\
&\mathcal{U}_1^{\mathrm{SF,TP}} = \mathcal{U}_2^{\mathrm{SF,TP}} = \frac{-B(\tilde{R}_b)\tilde{\phi}_b^2\mathcal{L}_{\mathrm{SF}b}}{1 + B(\tilde{R}_b)\tilde{\phi}_b\mathcal{L}_{\mathrm{SF}b}}, \quad b = 1 \text{ or } 2;\\
&\mathcal{U}_1^{\mathrm{TR,TP}} = \mathcal{U}_2^{\mathrm{TR,TP}} = \quad b = 1 \text{ or } 2;\\
&\qquad = \frac{B(\tilde{R}_b)\left[-\tilde{\phi}_b^2\mathcal{L}_{\mathrm{TR}b} + \tilde{\phi}_b - \tilde{\phi}_b(\tilde{\phi}_b\tilde{R}_b)^{(\nu-1)/\nu}\right]}{1 + B(\tilde{R}_b)\tilde{\phi}_b\mathcal{L}_{\mathrm{TR}b}},
\end{aligned} \tag{15}$$

with

$$\begin{aligned}
&B(\tilde{R}_b) = \nu A_\nu^{1/\nu}\tilde{R}_b^{(\nu-1)/\nu}, \quad b = 1 \text{ or } 2;\\
&\tilde{\phi}_1(\tilde{t}) = \tilde{\phi}_2(\tilde{t}) = \frac{\tilde{f}/2}{\tilde{R}_b + \tilde{\eta}_{\mathrm{p}12} + \tilde{s}_b}, \quad b = 1 \text{ or } 2;\\
&\mathcal{L}_{\mathrm{SF}b} = \frac{\nu - 1}{(2\nu - 1)\left[\tilde{R}_b + \tilde{s}_b + \tilde{\eta}_{\mathrm{p}12}\right]\tilde{\phi}_b^2} - \frac{1}{\tilde{\phi}_b}, \quad b = 1 \text{ or } 2;\\
&\mathcal{L}_{\mathrm{TR}b} = \frac{\tilde{\phi}_b^{-(1+\nu)/\nu}\tilde{R}_b^{(\nu-1)/\nu}}{\tilde{R}_b + \tilde{s}_b + \tilde{\eta}_{\mathrm{p}12}}\left[\frac{\nu - 1}{2\nu - 1}\tilde{\phi}_b\tilde{R}_b - \tilde{f}/2\right],\\
&b = 1 \text{ or } 2.
\end{aligned} \tag{16}$$

When the translocation process for the short branch 1 is in the PP stage and the long branch 2 is still in the propagation stage, i.e. the PP1–TP2 stage, as depicted in panel (b) of figure 1, mixture of different regimes of SS, SF and TR may occur. Therefore, the equations of motion for the tension front location for branches 1 and 2, when the translocation process for both branches is in the SS regime, i.e. the SS1–SS2 regime, are

$$\begin{aligned}
\dot{\tilde{R}}_1 &= -\tilde{\phi}_1;\\
\dot{\tilde{R}}_2 &= \frac{B(\tilde{R}_2)\tilde{\phi}_2}{1 - B(\tilde{R}_2)},
\end{aligned} \tag{17}$$

where $\tilde{\phi}_1 = \tilde{\phi}_2 = \tilde{\phi}$. Hereafter, for the cases where both branches are traversing the nanopore, we use $\tilde{\phi}$ instead of $\tilde{\phi}_1$ and $\tilde{\phi}_2$ as they are equal, and

$$\tilde{\phi} = \frac{\tilde{f}}{\tilde{R}_1 + \tilde{R}_2 + \tilde{s}_1 + \tilde{s}_2 + 2\tilde{\eta}_{\mathrm{p}12}}, \tag{18}$$

is the monomer flux for each branch.

For the PP1–TP2 stage, which is depicted in panel (b) of figure 1, when the translocation process is in the SS regime for short chain 1 and in the SF regime for the long branch 2, i.e. the SS1–SF2 regime, the equations of motion for $\tilde{R}_1$ and $\tilde{R}_2$ are coupled to each other as

$$\begin{aligned}
\dot{\tilde{R}}_1 &= -\tilde{\phi}, \qquad \mathrm{SS1\ regime;}\\
\dot{\tilde{R}}_1 + G_2\dot{\tilde{R}}_2 &= H_2, \qquad \mathrm{SF2\ regime.}
\end{aligned} \tag{19}$$

When the translocation process is in the SS regime for short chain 1 and in the TR regime for the long branch 2, i.e. the SS1–TR2 regime, the coupled equations of motion for $\tilde{R}_1$ and $\tilde{R}_2$ are

$$\begin{aligned}
\dot{\tilde{R}}_1 &= -\tilde{\phi}, \quad \mathrm{SS1\ regime;}\\
\dot{\tilde{R}}_1 + \mathbb{G}_2\dot{\tilde{R}}_2 &= \mathbb{H}_2, \quad \mathrm{TR2\ regime.}
\end{aligned} \tag{20}$$

When the translocation process is in the SF regime for short chain 1 and in the SS regime for the long branch 2, i.e. in the SF1–SS2 regime, the coupled equations of motion for $\tilde{R}_1$ and $\tilde{R}_2$ are

$$\begin{aligned}\dot{\tilde{R}}_1 + \dot{\tilde{R}}_2\frac{\mathcal{F}-1}{\mathcal{F}} &= \frac{(1-2\mathcal{F})\tilde{\phi}}{\mathcal{F}}, \quad \text{SF1 regime;}\\ \dot{\tilde{R}}_2 &= \frac{B(\tilde{R}_2)\tilde{\phi}}{1-B(\tilde{R}_2)}, \quad \text{SS2 regime.}\end{aligned} \tag{21}$$

When the translocation process is in the SF regime for both branches, i.e. in the SF1–SF2 regime, the coupled equations of motion for $\tilde{R}_1$ and $\tilde{R}_2$ are

$$\begin{aligned}\dot{\tilde{R}}_1 + \dot{\tilde{R}}_2\frac{\mathcal{F}-1}{\mathcal{F}} &= \frac{(1-2\mathcal{F})\tilde{\phi}}{\mathcal{F}}, \quad \text{SF1 regime;}\\ \dot{\tilde{R}}_1 + \dot{\tilde{R}}_2 G_2 &= H_2, \quad \text{SF2 regime.}\end{aligned} \tag{22}$$

When the translocation process is in the SF regime for short chain 1 and in the TR regime for the long branch 2, i.e. in the SF1–TR2 regime, the coupled equations of motion for $\tilde{R}_1$ and $\tilde{R}_2$ are

$$\begin{aligned}\dot{\tilde{R}}_1 + \dot{\tilde{R}}_2\frac{\mathcal{F}-1}{\mathcal{F}} &= \frac{(1-2\mathcal{F})\tilde{\phi}}{\mathcal{F}}, \quad \text{SF1 regime;}\\ \dot{\tilde{R}}_1 + \dot{\tilde{R}}_2 \mathbb{G}_2 &= \mathbb{H}_2, \quad \text{TR2 regime.}\end{aligned} \tag{23}$$

For the TR1–SS2 regime, where the translocation process is in the TR regime for short chain 1 and in the SS regime for the long branch 2, the coupled equations of motion for $\tilde{R}_1$ and $\tilde{R}_2$ are

$$\begin{aligned}\dot{\tilde{R}}_1 + \dot{\tilde{R}}_2 G_1 &= H_1, \quad \text{TR1 regime;}\\ \dot{\tilde{R}}_2 &= \frac{B(\tilde{R}_2)\tilde{\phi}}{1-B(\tilde{R}_2)}, \quad \text{SS2 regime.}\end{aligned} \tag{24}$$

When the translocation process is in the TR regime for short chain 1 and in the SF regime for the long branch 2, i.e. in the TR1–SF2 regime, the coupled equations of motion for $\tilde{R}_1$ and $\tilde{R}_2$ are

$$\begin{aligned}\dot{\tilde{R}}_1 + \dot{\tilde{R}}_2 G_1 &= H_1, \quad \text{TR1 regime;}\\ \dot{\tilde{R}}_1 + \dot{\tilde{R}}_2 G_2 &= H_2, \quad \text{SF2 regime.}\end{aligned} \tag{25}$$

In the TR1–TR2 regime, where the translocation process is in the TR regime for both branches, the coupled equations of motion for $\tilde{R}_1$ and $\tilde{R}_2$ are

$$\begin{aligned}\dot{\tilde{R}}_1 + \dot{\tilde{R}}_2 G_1 &= H_1, \quad \text{TR1 regime;}\\ \dot{\tilde{R}}_1 + \dot{\tilde{R}}_2 \mathbb{G}_2 &= \mathbb{H}_2, \quad \text{TR2 regime.}\end{aligned} \tag{26}$$

In the above equations of motion, G_b, H_b, $\mathbb{G}_2$, $\mathbb{H}_2$ and $\mathcal{F}$ are given by

$$\begin{aligned}G_b &= \frac{B(\tilde{R}_b)\mathcal{F}-1}{B(\tilde{R}_b)(\mathcal{F}-1)}, \quad b=1,2;\\ H_b &= \frac{B(\tilde{R}_b)(1-2\mathcal{F})\tilde{\phi}}{B(\tilde{R}_b)(\mathcal{F}-1)}, \quad b=1,2;\\ \mathbb{G}_2 &= \frac{1+(\mathcal{F}-1)\tilde{\phi}\tilde{R}_2 - B^{-1}(\tilde{R}_2)\,(\tilde{\phi}\tilde{R}_2)^{(1-\nu)/\nu}}{(\mathcal{F}-1)\tilde{\phi}\tilde{R}_2};\\ \mathbb{H}_2 &= \frac{2\tilde{\phi}(1-\mathcal{F})\tilde{\phi}\tilde{R}_2 - \tilde{\phi}(\tilde{\phi}\tilde{R}_2)^{(1-\nu)/\nu}}{(\mathcal{F}-1)\tilde{\phi}\tilde{R}_2};\\ \mathcal{F} &= 1+\frac{1-\nu}{2\nu-1}\frac{1}{\tilde{f}}.\end{aligned} \tag{27}$$

When the translocation process for the short branch 1 terminates and only the long branch is traversing the nanopore, which is depicted in panels (c) and (d) in figure 1, as explained in the main text of the paper the monomer flux for the long branch is

$$\tilde{\phi}_2 = \frac{\tilde{f}}{\tilde{R}_2 + \tilde{s}_2 + N_{01} + \tilde{\eta}_{\mathrm{p2}}}. \tag{28}$$

In the τ_1-TP2 stage (figure 1(c)), where the translocation process has completed for the short chain 1 and is in the PP stage for the long branch 2, the equations of motion for $\tilde{R}_2$ in the SS, SF and TR regimes, first, second and third lines in equation (29), respectively, are

$$\begin{aligned}\dot{\tilde{R}}_2 &= \frac{B(\tilde{R}_2)\tilde{\phi}_2}{1-B(\tilde{R}_2)}, \quad \text{SS2 regime;}\\ \dot{\tilde{R}}_2 &= \frac{B(\tilde{R}_2)\tilde{\phi}_2\mathcal{F}}{1-B(\tilde{R}_2)\mathcal{F}}, \quad \text{SF2 regime;}\\ \dot{\tilde{R}}_2 &= \frac{B(\tilde{R}_2)\left[-\tilde{\phi}_2(\tilde{\phi}_2\tilde{R}_2)^{(2\nu-1)/\nu}(1-\mathcal{F})+\tilde{\phi}_2\right]}{1+B(\tilde{R}_2)(\tilde{\phi}_2\tilde{R}_2)^{(\nu-1)/\nu}\left[\tilde{\phi}_2\tilde{R}_2(1-\mathcal{F})-1\right]},\\ &\qquad \text{TR2 regime.}\end{aligned} \tag{29}$$

In the τ_1-PP2 stage (figure 1(d)), where the translocation process has been completed for the short chain 1 and is in the PP stage for the long branch 2, the equations of motion for $\tilde{R}_2$ in the SS, SF and TR regimes, first, second and third lines in equation (30), respectively, are

$$\begin{aligned}\dot{\tilde{R}}_2 &= -\tilde{\phi}_2, \quad \text{SS2 regime;}\\ \dot{\tilde{R}}_2 &= -\tilde{\phi}_2, \quad \text{SF2 regime;}\\ \dot{\tilde{R}}_2 &= \frac{-(\tilde{\phi}_2\tilde{R}_2)^{(2\nu-1)/\nu}(1-\mathcal{F})+\tilde{\phi}_2}{(\tilde{\phi}_2\tilde{R}_2)^{(\nu-1)/\nu}\left[\tilde{\phi}_2\tilde{R}_2(1-\mathcal{F})-1\right]}, \quad \text{TR2 regime.}\end{aligned} \tag{30}$$

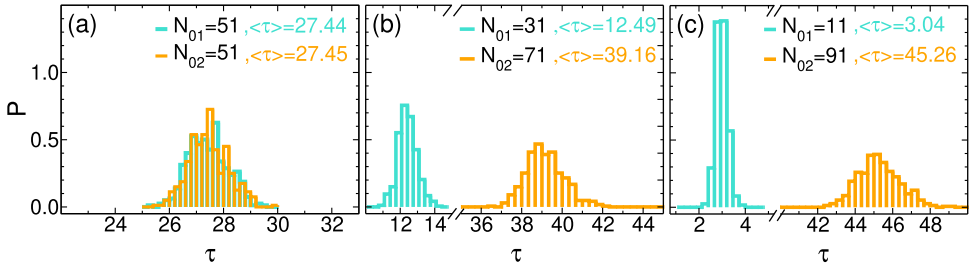

Figure 5. (a) The probability distribution of the translocation time, $P(\tau)$, for both branches of a folded polymer chain with total contour length of $N_0 = 101$, as a function of the translocation time τ when the folding is symmetric and the contour length of both branches are the same as $N_{01} = N_{02} = 51$. Panels (b) and (c) are the same as panel (a) but for asymmetrical folded polymer with different sets for the contour lengths of the branches $N_{01} = 31$ and $N_{02} = 71$, and $N_{01} = 11$ and $N_{02} = 91$, respectively. All data are from MD simulations.

Appendix B. Molecular dynamics simulations

As mentioned in the main text of the paper, to examine the validity of the theory we have performed extensive MD simulations of a folded polymer pulled through a pore by the monomer separating the two folded branches with $N_{01} \leqslant N_{02}$ monomers. This appendix presents the MD simulation method in detail. We have employed Langevin dynamics simulations using the LAMMPS package [58]. The polymer chain is modeled as a coarse-grained self-avoiding bead-spring chain, with each bead representing a monomer. The successive beads are connected by the finitely extensible nonlinear elastic (FENE) spring interaction given by

$$U_{\rm FENE}(r) = -\frac{kR_0^2}{2}\ln\left(1-\frac{r^2}{R_0^2}\right), \tag{31}$$

where k is the spring constant and R_0 is the maximum bond length. The excluded volume interaction between any two beads, and between a polymer bead and the pore particles is given by a repulsive Lennard-Jones (LJ) interaction

$$U_{\rm LJ}(r) = \begin{cases} 4\epsilon\left[\left(\frac{\sigma}{r}\right)^{12} - \left(\frac{\sigma}{r}\right)^{6}\right] + \epsilon, & \text{if } r < r_{\rm c}; \\ 0, & \text{if } r \geqslant r_{\rm c}, \end{cases} \tag{32}$$

where r is the distance between two beads, ϵ is the interaction strength and σ is the effective diameter of each bead. The cut-off radius is $r_{\rm c} = 2^{1/6}\sigma$. The Langevin equation for each ith particle of the system is solved as

$$m\ddot{\vec{r}}_i = -\vec{\nabla}(U_{\rm LJ} + U_{\rm FENE}) + \vec{f} + \vec{F}_i^F + \vec{F}_i^R, \tag{33}$$

where each polymer bead experiences conservative, frictional and random forces. The frictional force $\vec{F}_i^F = -\eta\vec{v}_i$, where $\vec{v}_i$ is the monomer velocity, η is the solvent friction coefficient, $\vec{f}$ is the external pulling force acting on the monomer being pulled, and $\vec{F}_i^R$ is the random force with zero mean $\langle\vec{F}_i^R(t)\rangle = 0$ which satisfies the fluctuation–dissipation relation, and $\langle\vec{F}_i^R(t)\cdot\vec{F}_j^R(t')\rangle = 6\eta k_{\rm B}T\delta_{ij}\delta(t-t')$ indicating that the random force is δ-correlated white noise. The parameters of our MD simulations in LJ units have been chosen as $\sigma = 1, \epsilon = 1, R_0 = 1.5\sigma, k = 30$ and $\eta = 0.7$. Here the magnitude of the external driving force is chosen as $f = 100$, and $k_{\rm B}T = 1.2$. In our model, the mass of each bead m is about 936 amu, its size $\sigma = 1.5$ nm corresponds approximately to the Kuhn length of a single-stranded DNA, and the interaction strength ϵ is 3.39×10^{-21} J at room temperature ($T = 295$ K). In LJ units, the time and force scales are 32.1 ps and 2.3 pN, respectively [13, 18]. The time step for the integration of the Langevin equation has been chosen as $\mathrm{d}t = 0.005$ (in LJ units) during the equilibration of the system and 0.0005 for the actual translocation process. It should be mentioned that the width of the pore is small and only one monomer for a linear chain or two monomers for a folded polymer can be inside the nanopore.

As schematically shown in figure 1, we consider a chain of an odd number of beads, $N_0 = 101$ with the pulled bead connecting the two branches placed at the pore. Here we consider folded chains with three different branch lengths of 51:51, 31:71 and 11:91. At the beginning of the simulations the folded polymer is carefully equilibrated with the pulled bead fixed at the pore. Then the constraint is removed and the external pulling force $\vec{f}$ starts acting on the bead from *cis* toward the *trans* side. As mentioned in the theory section the pulling force is strong enough such that the chain is essentially straightened on the *trans* side. Translocation time is recorded separately for the short and long segments. Our MD data here have been averaged over 400–500 independent runs.

Appendix C. Monomer velocities

This appendix presents additional data for the monomer velocities from the MD simulations (averaged over 400–500 successful translocation runs). In figure 4(a) the velocities of the individual monomers for the polymer branches, $v(m)$, have been plotted as a function of the normalized monomer index, m/N_{02}, at different moments of the translocation process $t =$ 2–20 for the symmetric folded chain with $N_{01} = N_{02} = 51$. The solid lines present the monomer velocities of the branch 1, while open symbols show the velocities for the branch 2. Panels (b) and (c) are the same as panel (a) but for an asymmetric folded polymer chain with branch contour lengths $N_{01} = 31$ and $N_{02} = 71$, and $N_{01} = 11$ and $N_{02} = 91$, respectively. In panel (b) the data are presented during $t =$ 2–28 and in panel (c) during $t =$ 1–36. Here, the individual monomer velocities have been averaged in the direction of the driving force, i.e. horizontal direction from the *cis* to the *trans* side. As can be seen in panel (a) for the symmetric 51:51 folded chain, the

monomer velocities for both branches are the same, and the TP occurs in an identical manner for both branches. At each moment, the velocities of the monomers for both branches that have already moved to the *trans* side have the same and constant value due to the strong pulling force. For the monomer beads which are in the *cis* side, there is a drop in velocity during the TP1–TP2 stage along both the chain branches and the velocity is zero for the non-mobile equilibrium part of the branches. In panels (b) and (c) as time passes, the TP1 of the short branch N_{01} ends and the PP1 stage starts. For example in panel (b) the interval $5 < t < 15$ is the transient window from TP1 to PP1 stage for the short branch, while the long one still is in its TP2 stage and the tension is still propagating along its backbone on the *cis* side. In the PP2 stage, as time progresses, the monomers' velocity of the long branch on the *cis* side sub-branch increases and finally becomes equal to that of the *trans* side sub-branch. Moreover, in all three panels (a), (b) and (c) the velocities of the individual monomers of both branches coincide with each other. This tells us that the equal monomer flux assumption in the IFTP theory is correct.

Appendix D. Translocation time distributions

This appendix presents the probability distributions of the translocation time, $P(\tau)$, for the folded polymer with various branched contour lengths using MD simulations. In panel (a) of figure 5 the probability distribution of the translocation time for both branches of the folded polymer chain with contour length of $N_0 = 101$, has been plotted as a function of the translocation time τ when the folding is symmetric and the contour lengths of both branches are the same as $N_{01} = N_{02} = 51$. Panels (b) and (c) are the same as panel (a) but for different sets for the contour lengths of the branches $N_{01} = 31$ and $N_{02} = 71$, and $N_{01} = 11$ and $N_{02} = 91$, respectively. When the folded chain becomes more asymmetrical, i.e. the contour length of one branch gets shorter and in contrast the other one becomes longer, the probability distributions for different branches are separated more from each other. As can be seen in figure 5(c) the separation is more pronounced than panel (b). Moreover, for shorter branch the width of the probability distribution is narrower due to the decrease in the spatial fluctuations of the branch configurations.

ORCID iDs

Bappa Ghosh https://orcid.org/0000-0002-4054-0859
Jalal Sarabadani https://orcid.org/0000-0002-4099-1537
Srabanti Chaudhury https://orcid.org/0000-0001-6718-8886
Tapio Ala-Nissila https://orcid.org/0000-0002-3210-3181

References

[1] Akeson M, Branton D, Kasianowicz J J, Brandin E and Deamer D W 1999 *Biophys. J.* **77** 3227
[2] Lingappa V R, Chaidez J, Yost C S and Hedgpeth J 1984 *Proc. Natl Acad. Sci.* **81** 456
[3] Turner S W P, Cabodi M and Craighead H G 2002 *Phys. Rev. Lett.* **88** 128103
[4] Chang D C 1992 *Guide to Electroporation and Electrofusion* (New York: Academic)
[5] Kasianowicz J J, Brandin E, Branton D and Deamer D W 1996 *Proc. Natl Acad. Sci.* **93** 13770
[6] Meller A, Nivon L and Branton D 2001 *Phys. Rev. Lett.* **86** 3435
[7] Sung W and Park P J 1996 *Phys. Rev. Lett.* **77** 783
[8] Muthukumar M 1999 *J. Chem. Phys.* **111** 10371
[9] Muthukumar M 2003 *J. Chem. Phys.* **118** 5174
[10] Sakaue T 2007 *Phys. Rev.* E **76** 021803
[11] Sakaue T 2010 *Phys. Rev.* E **81** 041808
[12] Saito T and Sakaue T 2012 *Eur. Phys. J.* E **34** 135
[13] Ikonen T, Bhattacharya A, Ala-Nissila T and Sung W 2012 *Phys. Rev.* E **85** 051803
[14] Ikonen T, Bhattacharya A, Ala-Nissila T and Sung W 2012 *J. Chem. Phys.* **137** 085101
[15] Ikonen T, Bhattacharya A, Ala-Nissila T and Sung W 2013 *Europhys. Lett.* **103** 38001
[16] Ikonen T, Shin J, Sung W and Ala-Nissila T 2012 *J. Chem. Phys.* **136** 205104
[17] Palyulin V V, Ala-Nissila T and Metzler R 2014 *Soft Matter* **10** 9016
[18] Sarabadani J, Ikonen T and Ala-Nissila T 2014 *J. Chem. Phys.* **141** 214907
[19] Sarabadani T, Ikonen T and Ala-Nissila T 2015 *J. Chem. Phys.* **143** 074905
[20] Sarabadani J, Ghosh B, Chaudhury S and Ala-Nissila T 2017 *Europhys. Lett.* **120** 38004
[21] Sarabadani J, Ikonen T, Mökkönen H, Ala-Nissila T, Carson S and Wanunu M 2017 *Sci. Rep.* **7** 7423
[22] Sarabadani J and Ala-Nissila T 2018 *J. Phys.: Condens. Matter.* **30** 274002
[23] de Haan H W and Slater G W 2010 *Phys. Rev.* E **81** 051802
[24] de Haan H W and Slater G W 2012 *J. Chem. Phys.* **136** 204902
[25] Gauthier M G and Slater G W 2009 *Phys. Rev.* E **79** 021802
[26] Cohen J A, Chaudhuri A and Golestanian R 2011 *J. Chem. Phys.* **107** 238102
[27] Cohen J A, Chaudhuri A and Golestanian R 2012 *Phys. Rev.* X **2** 021002
[28] Cohen J A, Chaudhuri A and Golestanian R 2012 *J. Chem. Phys.* **137** 204911
[29] Luo K, Ala-Nissila T, Ying S-C and Bhattacharya A 2008 *Phys. Rev. Rett.* **100** 058101
[30] Sigalov G, Comer J, Timp G and Aksimentiev A 2008 *Nano Lett.* **8** 56
[31] Milchev A 2011 *J. Phys.: Condens. Matter.* **23** 103101
[32] Smith D E *et al* 2001 *Nature* **413** 748
[33] Keyser U F, Dekker N H, Dekker C and Lemay S G 2009 *Nat. Phys.* **5** 347
[34] Keyser U F *et al* 2006 *Nat. Phys.* **2** 473
[35] Bulushev R D *et al* 2016 *Nano Lett.* **16** 7882
[36] Bulushev R D, Marion S and Radenovic A 2015 *Nano Lett.* **15** 7118
[37] Bulushev R D *et al* 2014 *Nano Lett.* **14** 6606
[38] Sischka A *et al* 2010 *J. Phys.: Condens. Matter.* **22** 454121
[39] Ritort F 2006 *J. Phys.: Condens. Matter.* **18** R531
[40] Ollila S T T, Luo K, Ala-Nissila T and Ying S-C 2009 *Eur. Phys. J.* E **28** 385
[41] Kantor Y and Kardar M 2004 *Phys. Rev.* E **69** 021806
[42] Huopaniemi I, Luo K, Ala-Nissila T and Ying S-C 2007 *Phys. Rev.* E **75** 061912
[43] Mathe J, Aksimentiev A, Nelson D R, Schulten K and Meller A 2005 *Proc. Natl Acad. Sci.* **102** 12377
[44] Dekker C 2007 *Nat. Nanotechnol.* **2** 209
[45] Storm A J, Chen J H, Ling X S, Zandbergen H W and Dekker C 2003 *Nat. Mater.* **2** 537

[46] Keyser U F, van der Does J, Dekker C and Dekker N H 2006 *Rev. Sci. Instrum.* **77** 105105
[47] Heng J B, Aksimentiev A, Ho C, Marks P, Grinkova Y V, Sligar S, Schulten K and Timp G 2005 *Nanao Lett.* **5** 1883
[48] Nakane J, Akeson M and Marziali A 2002 *Electrophoresis* **23** 2592
[49] Kasianowicz J J, Henrickson S E, Weetall H H and Robertson B 2001 *Nature* **73** 2268
[50] Bayley H and Cremer P S 2001 *Nature* **413** 226
[51] Bayley H and Martin C R 2000 *Chem. Rev.* **100** 2575
[52] Storm A J, Chen J H, Zandbergen H W, Joanny J-F and Dekker C 2005 *Nano Lett.* **5** 1193
[53] Storm A J, Chen J H, Zandbergen H W and Dekker C 2005 *Phys. Rev.* E **71** 051903
[54] Forrey C and Muthukumar M 2007 *J. Chem. Phys.* **127** 015102
[55] Kotsev S and Kolomeisky A B 2007 *J. Chem. Phys.* **127** 185103
[56] Rowghanian P and Grosberg A Y 2011 *J. Phys. Chem.* B **115** 14127
[57] Pincus P 1976 *Macromolecules* **9** 386
[58] Plimpton S 1995 *J. Comput. Phys.* **117** 1